Electronic Supplementary Material (ESI) for Physical Chemistry Chemical Physics.

Electronic Supplementary Information

for

Unified and Transferable Description of Dynamics for H_2 Dissociative Adsorption on Multiple Copper Surfaces via Machine Learning

Lingjun Zhu[#], Yaolong Zhang[#], Liang Zhang, Xueyao Zhou, and Bin Jiang[*]

Hefei National Laboratory for Physical Science at the Microscale, Key Laboratory of Surface and Interface Chemistry and Energy Catalysis of Anhui Higher Education Institutes, Department of Chemical Physics, University of Science and Technology of China, Hefei, Anhui 230026, China

# These authors contribute equally to this work

*: corresponding author: bjiangch@ustc.edu.cn

Supplementary Methods

A. Density Functional Theory Calculations

All density functional Theory (DFT) calculations in this work were performed with Vienna Ab Initio Simulation Package (VASP)[1,2], based on the projector augmented wave (PAW)[3] method and a plane-wave basis. We followed the seminal work[4-6] of Kroes and coworkers to set up slab models for H_2 adsorption on various copper surfaces. Specifically, each of three lowest index copper surfaces, namely Cu(111), Cu(100), and Cu(110), was modeled by a periodic (2×2) supercell, with a vacuum spacing of 15 Å in the Z direction. The bottom two layers of a four-layer slab were fixed at their bulk lattice positions for Cu(111) and Cu(100), while two uppermost layers were allowed to relax (namely 8 out of 16 surface atoms are movable per cell). Cu(110) was modeled by a five-layer slab (20 atoms) with three uppermost layers (12 atoms) relaxed. We also performed DFT calculations for H_2+Cu(211) in order to check the transferability of our potential energy surface (PES). For this stepped surface, a (1×2) supercell and ten-layer thick slab (20 Cu atoms) was constructed with the bottom four layers fixed and the same vacuum spacing. Additionally, to capture the variation of Cu-Cu interactions, Cu bulk structures were modeled in a 2×2×2 supercell containing 32 Cu atoms.

The exchange-correlation effects were described within the generalized gradient approximation (GGA)[7] using the optPBE-vdW[8] density functional (DF). This DF has shown to perform comparably well as a specific reaction parameter (SRP)[4] DF (well-known as SRP48[9]) that was fit to reproduce experimental sticking probabilities for H_2

dissociation on Cu(111). We chose the former because it intrinsically contains no empirical parameters and incorporates the van der Waals (vdW) interaction. For all H_2+Cu systems, 9×9×1 Γ-centered k-points were used to sample the Brillouin zone and the kinetic energy cutoff of plane-wave basis set was set to 400 eV. While for three-dimensional Cu bulk structures, 7×7×7 Γ-centered k-point mesh was adopted. Fermi smearing with a width of 0.1 eV was applied to account for partial occupancies of the metal near the Fermi level and warrant accurate total energies and forces. Transition state (TS) geometries and barrier heights for H_2 dissociation on various copper surfaces were identified by the dimer[10] method, which were all confirmed with a single imaginary frequency corresponding to the H-H stretching motion. We emphasize that these above settings are able to converge barrier heights well, as carefully checked by Kroes and coworkers in their work[4-6].

B. Embedded Atom Neural Network Representation

We used a physically inspired embedded atom neural network (EANN) approach[11] to learn diverse data points extracted from different surface slab models for H_2+Cu and Cu bulk structures in a uniform way. Analogous to the well-known embedded atom method (EAM)[12], the total energy of the system is decomposed into the embedded atomic energy, which is described in the EANN framework by an atomic NN as a function of embedded density.

$$E = \sum_{i=1}^{N} E_i = \sum_{i=1}^{N} NN_i(\boldsymbol{\rho}^i) . \qquad (1.)$$

Here $\boldsymbol{\rho}^i$ is the embedded density vector whose components represent the local electron density provided by the near atoms surrounding the central atom. Each component of

$\boldsymbol{\rho}^i$ can be obtained in the following way,

$$\rho^i_{L,\alpha,r_s} = \sum_{l_x,l_y,l_z}^{l_x+l_y+l_z=L} \frac{L!}{l_x!l_y!l_z!} \left(\sum_{j=1}^{n_{atom}} c_j \varphi^{\alpha,r_s}_{l_x,l_y,l_z}(\mathbf{r}^{ij})\right)^2, \quad (2.)$$

where Gaussian type like orbitals are centered at the neighboring atoms (n_{atom} in total),

$$\varphi^{\alpha,r_s}_{l_x,l_y,l_z}(\mathbf{r}^{ij}) = x_j^{\,l_x} y_j^{\,l_y} z_j^{\,l_z} exp(-\alpha|r - r_s|^2), \quad (3.)$$

with $\mathbf{r}^{ij} = (x, y, z)$ being the Cartesian coordinates of the embedded atom *i* relative to atom *j*, *r* being the distance between them, l_x, l_y, and l_z being the angular momentum component projected on each axis and their sum being the total orbital angular momentum (L), α and r_s being the parameters that determine radial distributions of atomic orbitals. Note that this formulism mimics the computation of electron density from atomic orbitals in quantum chemistry and c_j can be regarded as the linear combination coefficient of an orbital of atom *j* that is element-dependent and optimized in the training process.

The key advantage of this EANN method is that the density-like descriptors given in Eq. (2) scale linearly with respect to the number of neighboring atoms, which outperforms conventional atomistic NN strategy based on atom centered symmetry functions involving explicit summation of angular terms. The accuracy and efficiency of this EANN model have been demonstrated in our recent publication[11].

Since our goal is to construct a unified PES for H_2 dissociation on multiple copper surfaces, for which the configuration space is quite large. We chose to explore the dynamically relevant region by ab initio molecular dynamics (AIMD) simulations and collect data points for training from AIMD trajectories[13]. To mimic experimental conditions[14], Cu surface slabs starting from their equilibrium geometries were

equilibrated at several target surface temperatures (T_s=300K, 600K, and 900K) for 4 ps with a time step of 1 fs. Those surface configurations and corresponding velocities of Cu atoms during the last 1 ps NVT simulations were randomly chosen, followed by subsequent AIMD simulations for molecule-surface collision[13]. At most 150 AIMD trajectories were integrated for each H_2+Cu system with a time step of 0.5 fs until the H_2 molecule was either dissociated or reflected (see the next subsection for the description of initial sampling of H_2 coordinates and momenta, and the criteria of stopping trajectories).

In total, ~45 thousand DFT points were generated by those AIMD trajectories for H_2 scattering from Cu(111), Cu(100), and Cu(110) surfaces. In addition, we found that it is beneficial to include a number of heavily-distorted Cu bulk structures to represent the bare surface moving at very high surface temperature. To this end, 3000 distorted Cu bulk structures were extracted from similar AIMD simulations at temperatures of 300, 600, 1000 K. Based on a highly-efficient force-based screening algorithm[13], we chose only those points with distinct atomic forces and dissimilar geometries, including 1013 configurations H_2 plus Cu(111)/Cu(100)/Cu(110) surface and 300 Cu bulk structures for fitting the EANN PES.

To reach an adequate representability of the EANN model, we chose L_{max}=2, r_c=6 Å, α=0.6 Å^{-2}, and Δr_s=0.58 Å, resulting in 33 density-like descriptors. Two hidden layer NNs with 50 neurons in each layer were used for H, while 60 neurons in each layer for Cu. The whole fitting data set was divided randomly into two subsets, namely training (90%) and validating (10%) sets. The former was used to optimize the parameters with

an efficient extreme learning machine Levenberge Marquart algorithm[15] and the later to validate the fit enabling early stopping. The overall root-mean-squared-error (RMSE) over training and validating sets was 3.5 meV for the EANN PES. To validate the transferability of the EANN PES, we also ran AIMD trajectories for H_2 dissociation on Cu(211), yielding ~7300 DFT points. A small fraction (322 points) among them were added into the data set trained with the same EANN architecture, which led to the EANN-w211 PES with a fitting RMSE of 2.9 meV.

C. Quasi-Classical Trajectory Calculations

Quasi-classical dynamics calculations were performed to obtain dissociative sticking probabilities (S_0) on movable surfaces, taking advantage of the analytic gradients provided by the EANN PES. The diatomic molecule was treated as a rotating oscillator, whose internal energy was determined by the Einstein–Brillouin–Keller (EBK) semiclassical method[16] with given vibrational and rotational quantum numbers v and j. The corresponding internal coordinates and conjugate momenta were sampled with a Monte Carlo procedure[17]. For a given nozzle temperature (T_n), v and j were sampled based on corresponding Boltzmann distributions. Following Kroes and coworkers[4], the rotational temperature of hydrogen molecule in the beam was assumed to be $0.8\times T_n$ to account for partially rotational cooling, while vibrational temperature was kept at T_n. In addition, different weights for ortho and para rotational states of H_2 and D_2 due to nuclear spin statistics were considered in the Boltzmann sampling, *e.g.* the ratios of ortho/para states are 3:1 and 2:1 for H_2 and D_2, respectively. More importantly, the translational velocity (or equivalently the incident energy) is related to

T_n in pure supersonic molecular beams[18-20], resulting in a wide velocity spread of the impinging molecules. In this work, instead of assigning a fixed incident energy, we randomly sampled the initial incident velocity in light of T_n-dependent velocity distributions fitted to experimental time-of-flight (TOF) data by Kroes and coworkers[4], taking the following form,

$$f(v,T_n)dv = Cv^3 \exp[-(v - v_0)^2 / \alpha^2]dv \quad (4)$$

where fitting parameters v_0 and α are listed in Table S1.

To sample atomic positions and velocities of surface atoms prior to molecular collision, NVT molecule dynamics simulations of the bare surface were run at a given surface temperature (T_s) with a time step of 0.5 fs and an Andersen thermostat. After equilibrium (typically over 3 ps), uncorrelated surface configurations were extracted from snapshots of NVT molecular dynamics with a random time interval. In the subsequent NVE simulations, initial molecular center was placed at 7.0 Å above the first surface layer (namely the average height of surface atoms in the first layer), with lateral coordinates (X, Y) randomly sampled in the supercell and orientation randomly chosen. Each trajectory was propagated with a time step of 0.1 fs using the velocity Verlet algorithm up to 4 ps, unless being terminated either as a reactive trajectory if the interatomic distance was larger than 2.25 Å or a scattered one if the molecule-surface separation was over 7.1 Å and with its momentum pointing away from the surface. S_0 can be calculated as $S_0=N_r/N_{tot}$, where N_r represents the number of reactive trajectories, and N_{tot} is the total number of trajectories. In this work, we run as many as one million trajectories so as to warrant sufficiently good statistics in the entire energy range of

interest.

D. Quantum Dynamics Calculations

While it is impossible to include all surface DOFs, quantum dynamics (QD) calculations were used in this work to validate the QCT results on the static surface. This six-dimensional (6D) quantum wavepacket method has been well documented in our earlier work[21] and will be only briefly outlined here. Taking the H_2+Cu(111) system as an example, the quantum wave packet is represented by six Jacobi coordinates, as illustrated in Fig. S1. The quantum Hamiltonian can be written as,

$$\hat{H} = -\frac{1}{2M}\left(\frac{\partial^2}{\partial Z^2} + \frac{1}{\sin^2\gamma}\frac{\partial^2}{\partial u^2} + \frac{1}{\sin^2\gamma}\frac{\partial^2}{\partial v^2} - \frac{2\cos\gamma}{\sin^2\gamma}\frac{\partial^2}{\partial u \partial v}\right) - \frac{1}{2\mu}\frac{\partial^2}{\partial r^2} + \frac{\hat{j}^2}{2\mu r^2} + \hat{V}(Z,u,v,r,\theta,\phi), \quad (5)$$

where Z and (X, Y) correspond to perpendicular and parallel translation of the molecule, γ is the skew angle between two lattice vectors (u, v), M is the molecular mass, μ is the reduced mass of H_2 (or D_2), $\hat{j}$ is the molecular angular momentum, r is the inter-nuclear distance, θ and ϕ are angular coordinates represent the orientation with respect to the surface normal and surface plane, $\hat{V}(\mathbf{q})$ is the PES on a static surface.

The wave function is expanded by the radial and rotational basis functions. Specifically, sine basis functions are used for the translational coordinate Z,[22] which is divided into the interaction and asymptotic regions, in order to take advantage of an L grid saving scheme[23]. Periodic Fourier functions are used for u and v. The vibrational basis along r consists of the reference vibrational eigenfunctions $\phi_n(r)$ for the one-dimensional reference Hamiltonian for the isolated molecule far from the surface. A

non-direct product FBR consisting of spherical harmonics $Y_j^{m_j}(\theta,\varphi)$ is employed to represent the angular wave function. The initial wave packet is placed in the gas-phase asymptote ($Z = Z_i$) as a product of a Gaussian wave packet in Z and initial rovibrational wavefunction of the molecule, then propagated using the split-operator method[24] and absorbing potential was imposed at the edges of the grid to avoid spurious reflections. The initial state-selected reaction probability (namely S_0 here) is obtained by evaluating the energy dependent reactive flux at a dividing surface.

To achieve numerical convergence in the case of H_2/D_2+Cu(111), the two dimensional unit cell (u, v) was covered by a 14 × 14 evenly spaced Fourier grid. 160 sine basis functions were used ranging from 1.0 to 16.0 bohr for Z with 45 basis functions in the interaction region. 8 vibrational basis functions for r were used in the asymptotic region, while 38 in interaction region ranging from 0.5 to 6.0 bohr. The rotational basis was determined by $j_{\max} = 30$, $m_{j_{\max}} = 20$. The imaginary absorbing potentials started in the range of Z between 13.0 and 16.0 bohr and r between 4.0 and 6.0 bohr, respectively. The dissociation flux was calculated on the dividing surface of $r = 3.5$ bohr. The wave packets were propagated for 15000 a.u. of time with a time step of 10 a.u. to converge dissociation probabilities.

Supplementary Results and Discussion

There have been extensive theoretical studies for H_2 dissociation on flat and stepped copper surfaces[4-6,9,25-34]. In Table S2, we compare currently calculated barrier heights and transition state geometries with earlier results using various DFs[4-6,26,32]. It

is generally believed that the barrier heights for H_2 dissociative adsorption would increase incrementally when calculated by PW91[35], SRP48[9], and optPBE-vdW[8] DFs, respectively. For example, Wijzenbroek *et al.* found that the optPBE-vdW DF increases the barrier height by ~0.08 eV on either Cu(111) or Cu(100)[5], compared to the prediction of SRP48.[32] On Cu(110), while no data were reported using SRP48, our calculated barrier height with optPBE-vdW is ~0.22 eV higher than the PW91 value given by Salin[26]. Note that our calculations, in which the top several layers are movable during the optimization of transition state, differ from all previous ones based on static surfaces. As a result, even using the same optPBE-vdW DF and slab models, in general, we predict ~0.04 eV lower energies for similar transition states than those reported by Wijzenbroek *et al.* on Cu(111) and Cu(100)[5], due probably to the lattice effect. Interestingly, we find a transition state on Cu(100) centered at the middle of a top site and a hollow site (t2h), which was absent and much lower in energy than that at the bridge site as commonly identified in previous work[5,32]. This barrier height (0.673 eV) on Cu(100) thus becomes very close to that (0.672 eV) on Cu(111). There are seven transition states for H_2 dissociation on Cu(211), as identified by Füchsel et al.[6] using SRP48 and us using optPBE-vdW, reflecting strong corrugation of this stepped surface. Somewhat surprisingly, three transition states out of seven, *i.e.* t1, t2, and t2b following the same labeling in Ref. 6, have lower activation energies predicted by optPBE-vdW than by SRP48. In addition, our results show that the minimum barrier on Cu(211) (0.615 eV) is even lower than the barrier on Cu(111), in contrast to the SRP48 results[6]. However, the maximum barrier on Cu(211) remains very high (0.818 eV), indicating

that the barrier distribution (mean barrier height) on Cu(211) is broader (higher) than that on Cu(111), consistent with previous experimental findings[6,36].

In support of our discussion in the main text, we present Figs. S2-S4 and Table S3. Fig. S2 compares the EANN PES with DFT energies in two-dimensions (2D) in terms of uniform grids in Z and r (see Fig. S1), representing minimum energy pathways for H_2 dissociation on Cu(111), Cu(100), Cu(110), and Cu(211), with molecular orientation fixed at that of the transition state. The overall agreement between the PES and DFT energies on the three lowest-index surfaces is excellent. Note that the DFT energies were computed at sparser grids so that the resulting contours seem less smooth. Even for Cu(211), where no data has been learned, the 2D EANN PES cut shows no unphysical holes and reproduces DFT contours satisfactorily. Table S3 further illustrates that all of seven transition states on this stepped surface can be found and reasonably well described on this EANN PES. By adding ~300 more points for H_2+Cu(211) from AIMD simulations, the barrier heights of seven transition states can be further improved. This is not possible for those conventional system-specific molecule-surface PESs.

Fig. S3 compares QCT and QD calculated S_0 curves for ground state H_2 and D_2 on Cu(111). Previous theoretical studies have shown that, for activated dissociation of H_2 on metal surfaces, the QCT method does perform well at incident energies above the classical barrier[34], yielding sufficiently accurate S_0 values (say 0.01 or higher) with more favorable costs. Here, Fig. S3 verifies that this good agreement between QCT and QD for H_2 dissociation on Cu(111) remains valid for S_0 value being as low as 10^{-5},

where the incident energy is below classical barrier. This result is also in accord with our recent finding with an old empirical 6D PES for the same system[37], indicating that this behavior is independent of the PESs used. This justifies the use of the QCT method throughout this work, which allows us to involve surface motion in a straightforward and efficient way.

In Fig. S4, we compare the S_0 curves of H_2 on Cu(110) with and without considering the velocity spread in molecular beams, as well as results taken from Ref. [26] using a 6D PW91 PES and neglecting the velocity spread[26]. The experiment data of Berger *et al*.[20] serve as benchmark. At the first glance, it seems like the PW91 results agree very well with experimental data. However, our results (and also previous studies on Cu(111)[4,27]) clearly point out that the neglect of velocity distributions will significantly decrease the computed S_0 values, due to the fact that the high energy component in molecular beams contributes dominantly to the overall reactivity. As a result, our results with the optPBE-vdW DF are supposed to be at present the most accurate theoretical predictions for this system.

References

1. Kresse, G. & Furthmuller, J. Efficiency of ab initio total energy calculations for metals and semiconductors using plane wave basis set. *Comp. Mater. Sci.* **6**, 15-50 (1996).
2. Kresse, G. & Furthmuller, J. Efficient iterative schemes for ab initio total-energy calculations using plane wave basis set. *Phys. Rev. B* **54**, 11169-11186 (1996).
3. Blöchl, P. E. Projector augmented-wave method. *Phys. Rev. B* **50**, 17953-17979 (1994).
4. Díaz, C., Pijper, E., Olsen, R. A., Busnengo, H. F., Auerbach, D. J. & Kroes, G.-J. Chemically accurate simulation of a prototypical surface reaction: H_2 dissociation on Cu(111). *Science* **326**, 832-834 (2009).
5. Wijzenbroek, M., Klein, D. M., Smits, B., Somers, M. F. & Kroes, G.-J. Performance of a non-Local van der Waals density functional on the dissociation of H_2 on metal surfaces. *J. Phys. Chem. A* **119**, 12146-12158 (2015).
6. Füchsel, G*., et al.* Anomalous dependence of the reactivity on the presence of steps: Dissociation of D_2 on Cu(211). *J. Phys. Chem. Lett.* **9**, 170-175 (2018).
7. Perdew, J. P., Burke, K. & Ernzerhof, M. Generalized gradient approximation made simple. *Phys. Rev. Lett.* **77**, 3865-3868 (1996).
8. Klimeš, J., Bowler, D. R. & Michaelides, A. Chemical accuracy for the van der Waals density functional. *J. Phys.: Condens. Matter* **22**, 022201 (2010).
9. Nattino, F., Díaz, C., Jackson, B. & Kroes, G.-J. Effect of surface motion on the rotational quadrupole alignment parameter of D_2 reacting on Cu(111). *Phys. Rev. Lett.* **108**, 236104 (2012).
10. Henkelman, G. & Jónsson, H. A dimer method for finding saddle points on high dimensional potential surfaces using only first derivatives. *J. Chem. Phys.* **111**, 7010-7022 (1999).
11. Zhang, Y., Hu, C. & Jiang, B. Embedded atom neural network potentials: Efficient and accurate machine learning with a physically inspired representation. *J. Phys. Chem. Lett.* **10**, 4962-4967 (2019).
12. Daw, M. S. & Baskes, M. I. Embedded-atom method: Derivation and application to impurities, surfaces, and other defects in metals. *Phys. Rev. B* **29**, 6443-6453 (1984).
13. Zhang, Y., Zhou, X. & Jiang, B. Bridging the gap between direct dynamics and globally accurate reactive potential energy surfaces using neural networks. *J. Phys. Chem. Lett.* **10**, 1185-1191 (2019).
14. Murphy, M. J. & Hodgson, A. Adsorption and desorption dynamics of H_2 and D_2 on Cu(111): The role of surface temperature and evidence for corrugation of the dissociation barrier. *J. Chem. Phys.* **108**, 4199-4211 (1998).
15. Zhang, Y.-l., Zhou, X.-y. & Jiang, B. Accelerating the construction of neural network potential energy surfaces: A fast hybrid training algorithm. *Chin. J. Chem. Phys.* **30**, 727-734 (2017).
16. Gutzwiller, M. C. *Chaos in Classical and Quantum Mechanics*. Springer (1990).
17. Peslherbe, G. H., Wang, H. & Hase, W. L. Monte Carlo sampling for classical trajectory simulations. *Adv. Chem. Phys.* **105**, 171-201 (1999).
18. Anger, G., Winkler, A. & Rendulic, K. D. Adsorption and desorption kinetics in the systems H2/Cu(111), H2/Cu(110) and H2/Cu(100). *Surf. Sci.* **220**, 1 (1989).
19. Berger, H. F., Leisch, M., Winkler, A. & Rendulic, K. D. A search for vibrational

contributions to the activated adsorption of H2 on copper. *Chem. Phys. Lett.* **175**, 425-428 (1990).

20. Berger, H. F. & Rendulic, K. D. An investigation of vibrationally assisted adsorption: the cases H2/Cu(110) and H2/Al(110). *Surf. Sci.* **253**, 325-333 (1991).
21. Jiang, B. & Guo, H. Six-dimensional quantum dynamics for dissociative chemisorption of H_2 and D_2 on Ag(111) on a permutation invariant potential energy surface. *Phys. Chem. Chem. Phys.* **16**, 24704-24715 (2014).
22. Colbert, D. T. & Miller, W. H. A novel discrete variable representation for quantum mechanical reactive scattering via the S-matrix Kohn method. *J. Chem. Phys.* **96**, 1982 (1992).
23. Zhang, D. H. & Zhang, J. Z. H. Accurate quantum calculations for the benchmark reaction H_2 +OH → H_2O + H in five-dimensional space: reaction probability for J=0. *J. Chem. Phys.* **99**, 5615-5618 (1993).
24. Flect Jr., J. A., Morris, J. R. & Feit, M. D. Time-dependent propagation of high energy laser beam through the atmosphere. *Appl. Phys.* **10**, 129 (1976).
25. Kroes, G. J., Pijper, E. & Salin, A. Dissociative chemisorption of H_2 on the Cu(110) surface: A quantum and quasiclassical dynamical study. *J. Chem. Phys.* **127**, 164722 (2007).
26. Salin, A. Theoretical study of hydrogen dissociative adsorption on the Cu(110) surface. *J. Chem. Phys.* **124**, 104704 (2006).
27. Diaz, C., Olsen, R. A., Auerbach, D. J. & Kroes, G.-J. Six-dimensional dynamics study of reactive and non reactive scattering of H_2 from Cu(111) using a chemically accurate potential energy surface. *Phys. Chem. Chem. Phys.* **12**, 6499-6519 (2010).
28. Kroes, G.-J. Towards chemically accurate simulation of molecule–surface reactions. *Phys. Chem. Chem. Phys.* **14**, 14966-14981 (2012).
29. Muzas, A. S., Juaristi, J. I., Alducin, M., Muiño, R. D., Kroes, G. J. & Díaz, C. Vibrational deexcitation and rotational excitation of H_2 and D_2 scattered from Cu(111): Adiabatic versus non-adiabatic dynamics. *J. Chem. Phys.* **137**, 064707 (2012).
30. Bonfanti, M., Somers, M. F., Díaz, C., Busnengo, H. F. & Kroes, G.-J. 7D Quantum Dynamics of H_2 Scattering from Cu(111): The Accuracy of the Phonon Sudden Approximation. *Z. Phys. Chem. (Muenchen, Ger.)* **227**, 1397-1420 (2013).
31. Marashdeh, A., Casolo, S., Sementa, L., Zacharias, H. & Kroes, G.-J. Surface temperature effects on dissociative chemisorption of H_2 on Cu(100). *J. Phys. Chem. C* **117**, 8851-8863 (2013).
32. Sementa, L.*, et al.* Reactive scattering of H2 from Cu(100): Comparison of dynamics calculations based on the specific reaction parameter approach to density functional theory with experiment. *J. Chem. Phys.* **138**, 044708 (2013).
33. Nattino, F.*, et al.* Dissociation and recombination of D2 on Cu(111): Ab initio molecular dynamics calculations and improved analysis of desorption experiments. *J. Chem. Phys.* **141**, 124705 (2014).
34. Kroes, G.-J. & Diaz, C. Quantum and classical dynamics of reactive scattering of H_2 from metal surfaces. *Chem. Soc. Rev.* **45**, 3658-3700 (2016).
35. Perdew, J. P.*, et al.* Atoms, molecules, solids, and surfaces: Applications of the generalized gradient approximation for exchange and correlation. *Phys. Rev. B* **46**, 6671-6687 (1992).
36. Kaufmann, S., Shuai, Q., Auerbach, D. J., Schwarzer, D. & Wodtke, A. M. Associative desorption of hydrogen isotopologues from copper surfaces: Characterization of two reaction

mechanisms. *J. Chem. Phys.* **148**, 194703 (2018).

37. Liu, Q., Zhang, L., Li, Y. & Jiang, B. Ring Polymer Molecular Dynamics in Gas–Surface Reactions: Inclusion of Quantum Effects Made Simple. *J. Phys. Chem. Lett.* **10**, 7475-7481 (2019).

38. Michelsen, H. A., Rettner, C. T., Auerbach, D. J. & Zare, R. N. Effect of rotation on the translational and vibrational energy dependence of the dissociative adsorption of D_2 on Cu(111). *J. Chem. Phys.* **98**, 8294-8307 (1993).

Table S1: Parameters of velocity distributions of incident beams in various experiments as described by Eq. (4) taken from Ref. 4. Note that the velocity distribution depends on the nozzle temperature in pure beam, as in Ref. 19 for H_2+Cu(111), Ref. 18 for H_2+Cu(100), and Ref. 20 for H_2+Cu(110), but on the velocity of the carrier gas in seeded beam at a fixed nozzle temperature, as in Ref. 38 for D_2+Cu(111).

$< E_i >$ [eV]	v_0 [m/s]	α [m/s]	T_n [K]
D_2+Cu(111)[38]			
0.369	3925	816	
0.485	4595	782	
0.653	5377	829	2100
0.723	5658	866	
0.837	6132	849	
H_2+Cu(111)/Cu(100)/Cu(110)[18-20]			
0.260	3500	1996	1205
0.310	3555	2342	1437
0.335	3380	2611	1553
0.348	3151	2819	1623
0.367	3219	2903	1711

Table S2: Barrier heights (E_a) and corresponding transition state geometries (see Fig. S1) for H_2 dissociation on multiple copper surfaces calculated by DFT with the optPBE-vdW DF in this work, and those derived from DFT-based PESs, using SRP48, PW91, and optPBE-vdW DFs, respectively. These earlier results were all based on frozen surface approximation but surface atoms were movable in our calculations.

		SRP48 or PW91			**optPBE-vdW**		
surface	**site**	E_a **(eV)**	r **(Å)**	Z **(Å)**	E_a **(eV)**	r **(Å)**	Z **(Å)**
Cu(111)	brg	0.636[a]	1.03	1.17	0.672(0.712[d])	1.04(1.05)	1.16(1.17)
Cu(100)	brg	0.742[a]	1.24	0.99	0.777(0.822[d])	1.18(1.24)	1.01(1.00)
	t2h	-	-	-	0.673	1.16	1.18
Cu(110)	brg	0.592[b]	1.17	0.86	0.812	1.20	0.89
Cu(211)	b1	0.727[c]	1.17	0.98	0.750	1.17	0.98
	b2	0.673[c]	1.06	0.89	0.714	1.06	0.89
	b3	0.726[c]	1.04	0.48	0.750	1.06	0.49
	b4	0.800[c]	1.04	0.17	0.818	1.06	0.15
	t1	0.694[c]	1.43	1.37	0.615	1.36	1.31
	t2	0.727[c]	1.13	0.26	0.686	1.12	0.31
	t2b	0.663[c]	1.41	1.31	0.615	1.36	1.31

[a]Data for Cu(111) and Cu(100) taken from Ref. 5 and Ref. 32 using SRP48 PES.

[b]Data for Cu(110) taken from Ref. 26 using PW91 DF.

[c]Data for Cu(211) taken from Ref. 6 using SRP48 DF.

[d]Data in brackets for Cu(111) and Cu(100) were taken from the optPBE-vdW PESs in Ref. 5.

Table S3: Barrier heights (E_a) and transition state geometries (r, Z) for EANN and EANN-w211 PESs for H_2 dissociation on Cu(111), Cu(100), Cu(110) above the best reactive site and on Cu(211) above all reactive sites.

		EANN PES			**EANN-w211 PES**		
surface	**site**	E_a **(eV)**	r **(Å)**	Z **(Å)**	E_a **(eV)**	r **(Å)**	Z **(Å)**
Cu(111)	brg	0.685	1.02	1.16	0.678	1.03	1.16
Cu(100)	t2h	0.683	1.15	1.16	0.689	1.18	1.17
Cu(110)	brg	0.799	1.23	0.87	0.821	1.19	0.89
	b1	0.730	1.20	0.95	0.753	1.17	0.98
	b2	0.770	1.18	1.00	0.718	1.07	0.90
	b3	0.808	1.05	0.44	0.754	1.07	0.48
Cu(211)	b4	0.881	1.11	0.24	0.822	1.05	0.15
	t1	0.632	1.40	1.29	0.616	1.37	1.30
	t2	0.746	1.06	0.30	0.692	1.12	0.32
	t2b	0.632	1.40	1.29	0.616	1.37	1.30

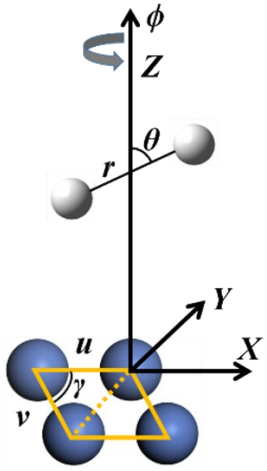

Fig. S1 Six coordinates defined in our quantum dynamical model for the H_2+Cu(111) system.

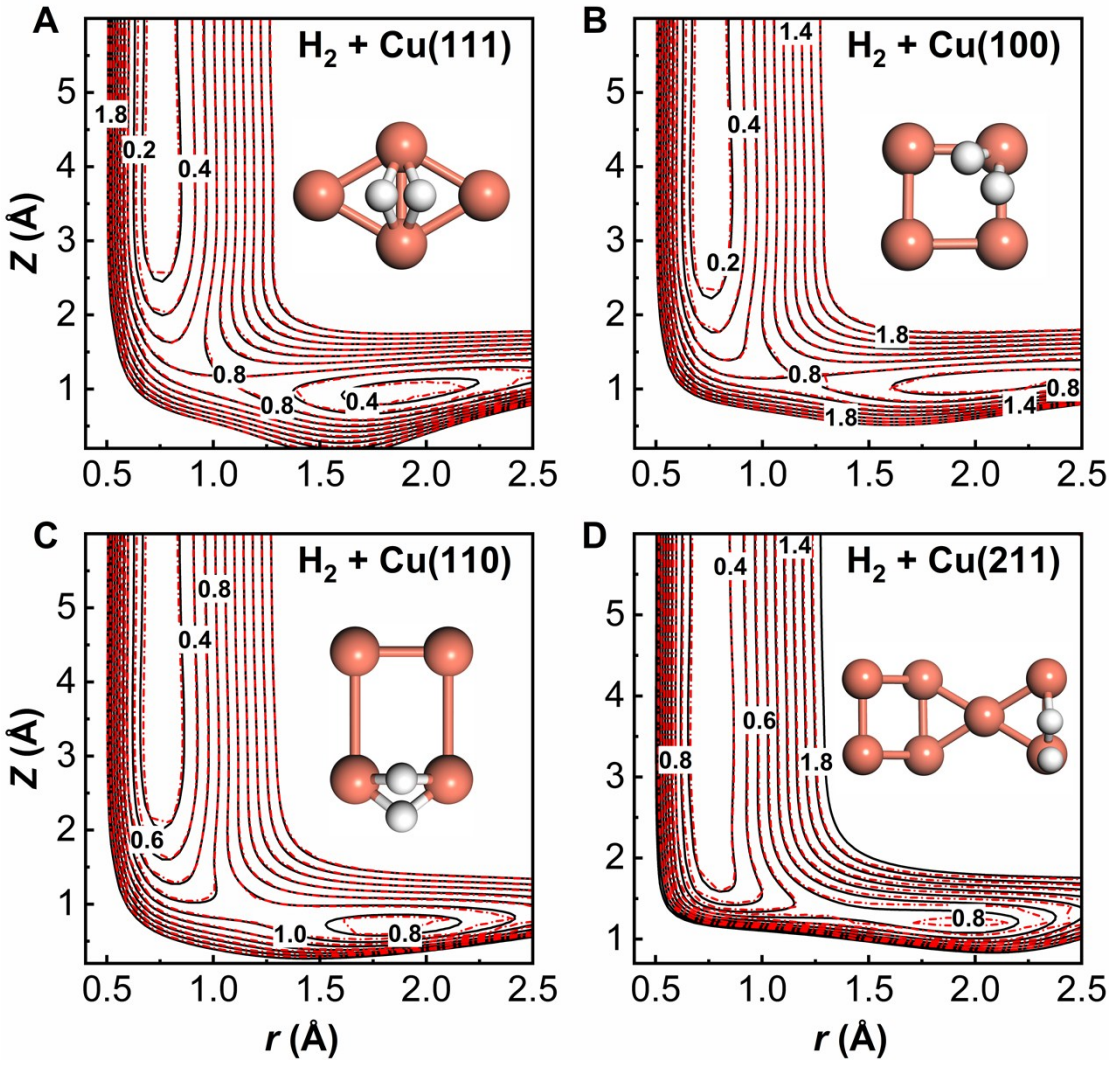

Fig. S2 Contour plots for (A) H_2+Cu(111), (B) H_2+Cu(100), (C) H_2+Cu(110), (D) H_2+Cu(211) systems obtained from the PES (solid lines) and DFT (dashed lines) calculations, as a function of *Z* and *r*, with molecular orientation fixed at that of the transition state geometry on each surface. Contour lines (energies in eV) have a spacing of 0.2 eV, giving the energies of EANN PES with solid black lines and the DFT energies with dash-dot red lines. The minimum energy transition state geometries of H_2 dissociation on Cu(111), Cu(100), Cu(110), and Cu(211) optimized by DFT calculations are also shown as insets.

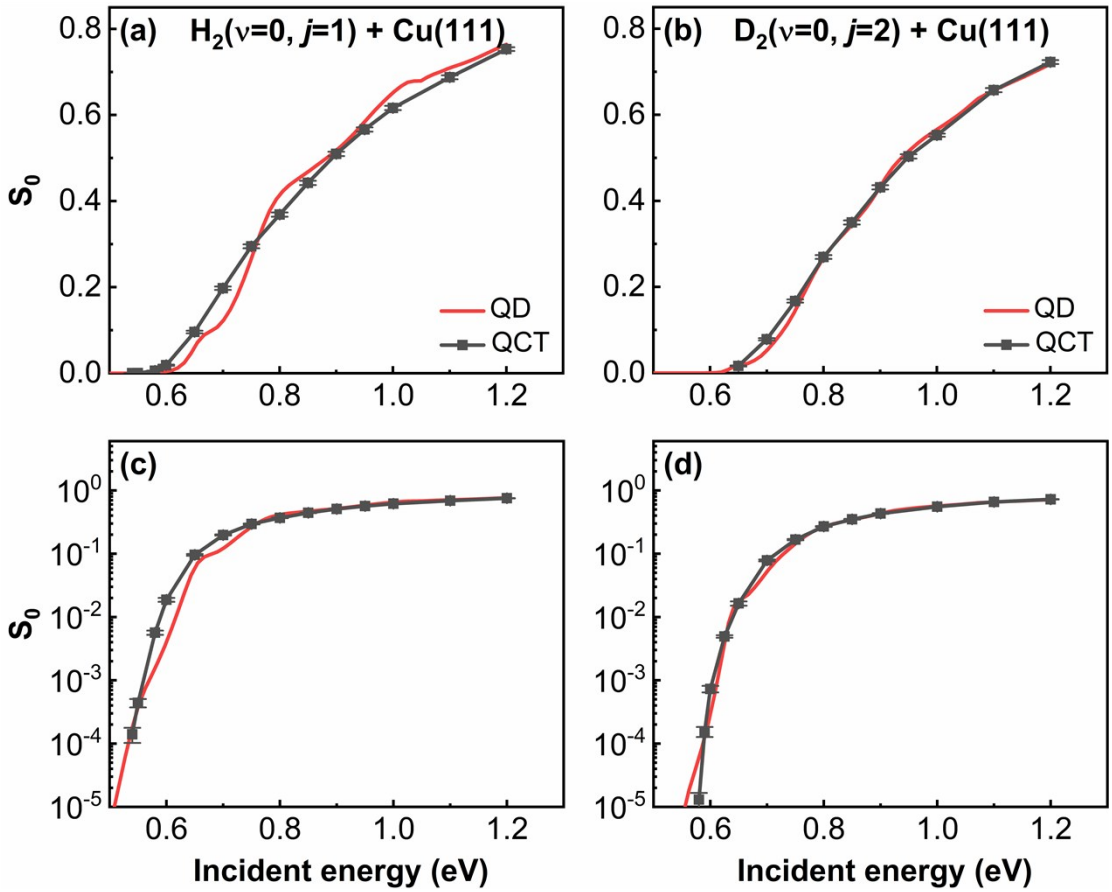

Fig. S3 Comparison of S_0 curves of H_2(v=0, j=1) (a, c) and D_2(v=0, j=2) (b, d) on Cu(111) computed with QCT (black symbols) and QD (red curves) methods on the EANN PES, shown in a linear scale (upper panels) and a logarithmic scale (lower panels), respectively.

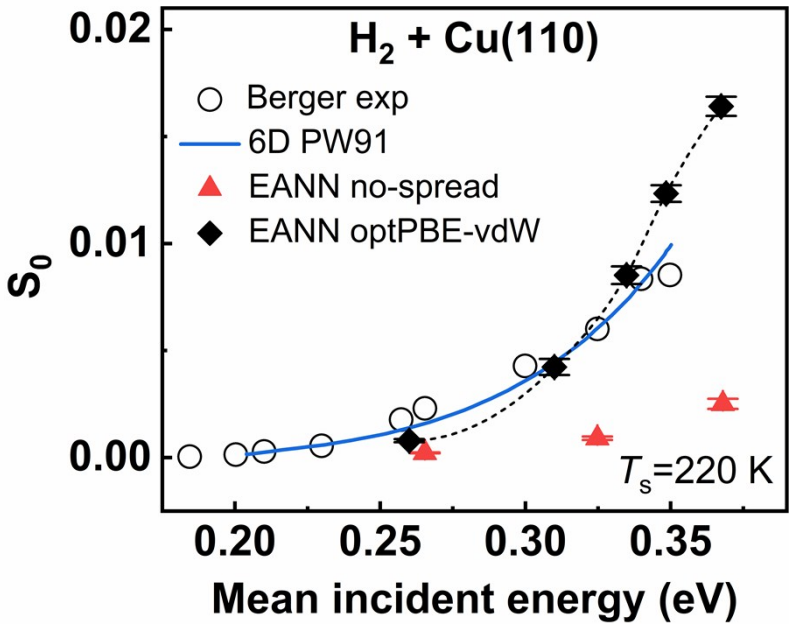

Fig. S4 Comparison of calculated H_2 sticking probabilities with (black diamond) or without (red triangle) velocity spread on the Cu(110) surface at T_s=220K, together with the result from Salin[26] using PW91 DF neglecting the velocity spread and the experiment data of Berger *et al*.[20]

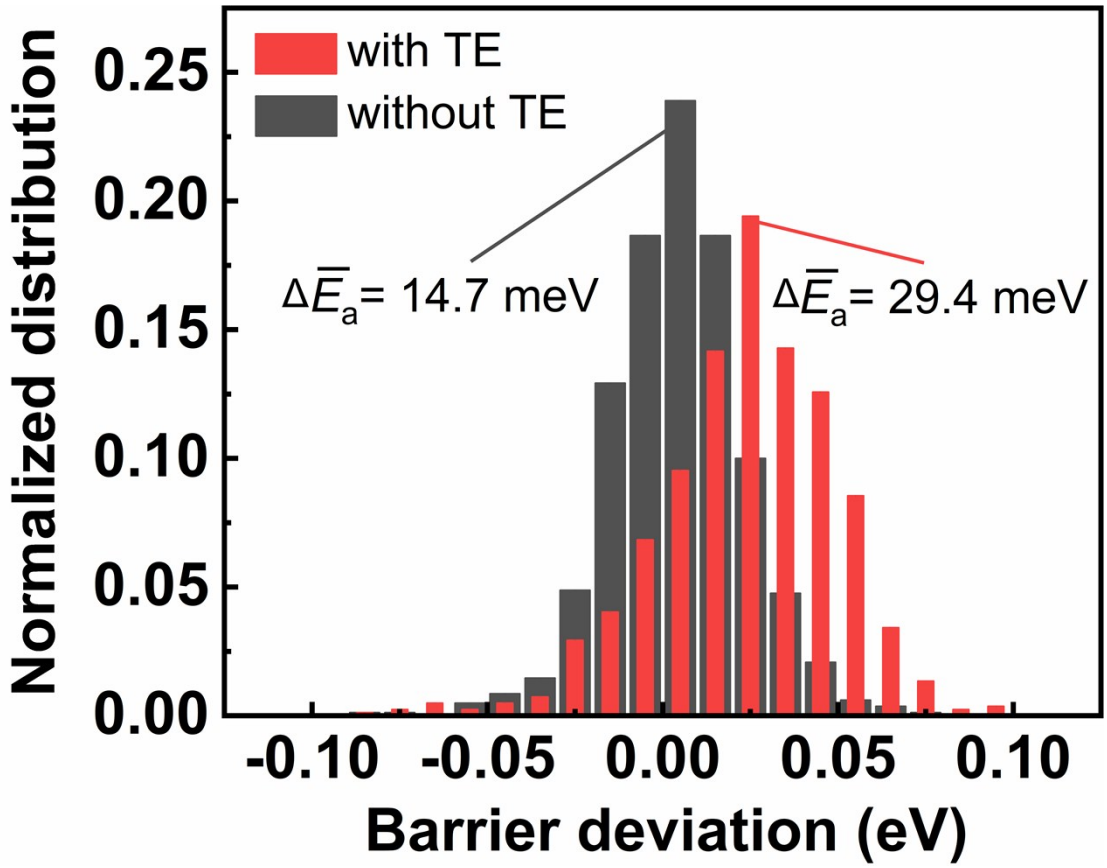

Fig. S5 Distributions of the deviations between DFT and EANN barrier heights for H_2 dissociation on Cu(111) with (red) and without (black) thermal expansion (TE) on a large number of surface structures at 900 K.